JOURNAL OF GUIDANCE, CONTROL, AND DYNAMICS
Vol. 22, No. 2, March–April 1999

Sensitivity of Trajectory Prediction in Air Traffic Management

Michael R. Jackson*
Honeywell Technology Center, Minneapolis, Minnesota 55418
Yiyuan J. Zhao†
University of Minnesota, Minneapolis, Minnesota 55455
and
Rhonda A. Slattery‡
NASA Ames Research Center, Moffett Field, California 94035

Trajectory prediction in air traffic management computes the most likely or the most desirable aircraft trajectories by using models of aircraft performance and atmospheric conditions, as well as measurements of aircraft states. In comparison, actual trajectories are obtained using feedback control from a pilot or autopilot to track flight objectives, while the aircraft flies through an actual atmosphere. This paper introduces the concept of closed-loop sensitivities, which are defined as differences between actual and computed trajectories per unit of modeling errors, in the presence of pilot/autopilot feedback controls. Modeling errors are expressed as uncertain parameters and/or uncertain functions. Pilot/autopilot control actions are approximated by nonlinear feedback control laws, designed with the method of feedback linearization. Both the aircraft equations of motion and the feedback control laws are linearized around computed reference trajectories, and these linearized equations are used to determine expressions for closed-loop terminal sensitivities. The proposed method is applied to the Center/Terminal Radar Approach Control (TRACON) Automation System as well as flight management systems.

Nomenclature

a	= speed of sound
C_D, C_L	= drag and lift coefficients, respectively
D	= aerodynamic drag
$\boldsymbol{d}(t)$	= uncertain time-varying disturbance
F	= aircraft dynamic equations
G	= pilot/autopilot feedback control laws
g	= gravitational acceleration
h_I, h_p	= inertial and pressure altitudes, respectively
L	= aerodynamic lift
M	= Mach number
$\mathcal{M}$	= generic error source
m	= aircraft mass
$\dot{m}_f$	= fuel flow rate
p	= static air pressure
$\boldsymbol{p}$	= uncertain parametric error
Q	= measurements of initial conditions
S	= aircraft reference area
s	= ground path distance to destination
T	= engine thrust
t	= time
$\boldsymbol{u}$	= control vector
V_{CAS}	= calibrated airspeed
V_g	= ground speed
V_t	= true airspeed
W_x, W_y, W_h	= wind components, east, north, and up, respectively
$\dot{W}_V$, $\dot{W}_\chi$, $\dot{W}_\gamma$	= wind acceleration components
$\boldsymbol{x}$	= state vector
$\boldsymbol{x}^*$	= reference trajectory state vector
x_I, y_I	= east and north positions, respectively
$\boldsymbol{z}$	= computed (predicted) trajectory
α_t	= angle of attack of the engines
γ_a, γ_I	= air-mass and inertial flight-path angles, respectively
κ	= throttle setting
μ	= bank angle
ρ	= air density
Φ	= state transition matrix
χ_a, χ_I	= air-mass and inertial velocity headings, respectively
ψ	= segment termination condition
$()_{d,p,x,u}$	= partial derivatives
$()_{\mathrm{sl}}$	= sea level conditions

Received April 2, 1998; revision received July 29, 1998; accepted for publication Aug. 7, 1998.

*Principal Research Scientist. E-mail: jackson@htc.honeywell.com. Member AIAA.

†Associate Professor, Department of Aerospace Engineering and Mechanics, 110 Union Street. E-mail: gyyz@aem.umn.edu. Senior Member AIAA.

‡Research Engineer; currently Systems Engineer, Wide Area Augmentation System, Raytheon Systems Company, 1801 Hughes Drive FU, Building 675, Mail Stop P334, Fullerton, CA 92834. Member AIAA.

Introduction

INCREASING nationwide air travel has severely burdened the current air traffic control (ATC) infrastructure and created a heavy workload for air traffic controllers. At the same time, rising fuel prices, airline competition, and environmental concerns have heightened the need to save fuel. It has become increasingly important to develop ATC automation systems to assist controllers in guaranteeing safety, increasing airport throughput, and reducing aircraft delays.

Over the last decade, researchers at NASA Ames Research Center have been developing an air traffic control automation tool called the Center/TRACON Automation System (CTAS).[1–5] CTAS can assist air traffic controllers in both en route (center) and terminal areas [terminal radar approach control (TRACON)] by providing computer-generated flight advisories. These advisories guarantee safe separation of aircraft and produce an expeditious flow of traffic.

CTAS includes two essential functions: trajectory synthesis and scheduling.[1] Trajectory synthesis first computes nominal flight trajectories for all aircraft within a region.[6–10] Based on estimated times of arrival and the range of achievable times derived from these computed trajectories, the scheduler generates an efficient landing order and landing times to minimize average aircraft delay and controller workload.[2,11–13] Next, trajectory synthesis recomputes the trajectories, iterating on speed, altitude, and lateral path as necessary to meet the scheduled landing times and to ensure separation among aircraft.[14,15] Finally, CTAS extracts advisories from the trajectories for each aircraft in terms of heading, speed, altitude, and top-of-descent location and displays the advisories to the controllers.

In addition, onboard flight management systems (FMS) use trajectory synthesis methods to develop optimal flight trajectories that

reduce fuel consumption.[8,16–20] Feedback guidance is employed to track the optimal trajectories.

For both CTAS and FMS, trajectory syntheses use models of aircraft performance, atmospheric conditions, and pilot techniques. On the other hand, actual aircraft are flown in real conditions where pilot or autopilot feedback control tracks certain features of computed trajectories. The differences between actual and computed trajectories reflect the accuracy of trajectory predictions. Knowledge of how trajectory prediction accuracy is sensitive to modeling errors is valuable to the designers and users of systems based on trajectory prediction.

In the past, both nonlinear simulations and flight tests were conducted to analyze the differences between actual and computed trajectories. Williams[21,22] and Williams and Knox[23] examined the effects of constant mismodeled winds and mismodeled idle thrust on computed trajectories by regenerating computed trajectories, as well as the effects on actual fuel and time penalties with a trajectory tracker. Scientists at Seagull Technology, Inc., have conducted several studies on aircraft trajectory prediction errors and the impact of the errors on the efficiency of air traffic flow[24–28] using Monte Carlo simulations. NASA and the Federal Aviation Administration have cooperatively conducted flight tests to investigate trajectory prediction accuracies and sources of errors using the NASA transport systems research vehicle and operating airline flights by United Airlines, Mesa Airlines, and Mark Air. The experiments were based out of the Denver Center during the fall of 1994 and 1995 as part of an evaluation of the CTAS Descent Advisor system. The results of these experiments are described in Refs. 29 and 30.

In other related work, Izumi[31] considered the effects of different trajectory generation algorithms on airport throughput and system efficiency. Chatterji et al.[32] studied the sensitivity of ground speed to atmospheric errors. Bolender[33] reported the variations in CTAS predictions of estimated times of arrival at the Denver Stapleton Airport and considered the inaccuracies in the radar measurements of ground speed and heading and wind variations as the causes of the observed variations. Williams and Green[34] described a research FMS developed at NASA Langley Research Center that includes four-dimensional trajectory tracking algorithms used to control an aircraft to a desired time of arrival. The method is based on computing a predicted error in arrival time and using feedback to control the arrival time. Morton[35] developed a method of studying trajectory dispersion with known control laws based on linearization of the dynamics and used the method to study booster vehicles with a terminal condition of fuel exhaustion.

This paper presents a method that can determine the effects of individual error sources on trajectory prediction accuracy. Specifically, a concept of closed-loop sensitivity is proposed, which measures the variations of trajectory differences with respect to individual modeling errors in the presence of pilot controls. Various modeling errors are described as uncertain parameters and/or uncertain functions. Pilot or autopilot feedback control actions are expressed as equality constraints. Equations of motion are linearized along a reference trajectory, whereas control variations are eliminated by using the linearized constraints. As a result, differences between actual and reference trajectories due to modeling errors are governed by a set of linear differential equations with time-varying coefficients. This set of linear equations is used to obtain expressions for closed-loop sensitivities. Numerical examples are then presented that describe the trajectory sensitivity for several different methods of feedback control during an aircraft descent.

This paper presents selected results from Ref. 36. Interested readers may contact the first author for a copy of that paper.

Problem Statement

Figure 1 shows a typical airline flight, along with the ATC facilities that are responsible during different portions of the flight.

A key component of CTAS is the trajectory synthesizer, which predicts the flight paths of all aircraft within a specified region. Figure 2 shows the environment of CTAS trajectory prediction, where sources of errors are shown in italics. A similar diagram can be drawn for FMS and is omitted for brevity. Because of various modeling errors, actual aircraft trajectories $\boldsymbol{x}$ are different from predicted (computed) trajectories $\boldsymbol{z}$.

An important factor in studying the trajectory differences is that pilots or autopilots follow certain features of computed trajectories. Therefore, a concept of closed-loop sensitivity is defined as the difference between the actual trajectory and the predicted trajectory per unit of an error source, in the presence of pilot or autopilot feedback control. If $\mathcal{M}$ represents a certain error source, closed-loop sensitivities can be stated symbolically as

$$\frac{\partial(\boldsymbol{x}-\boldsymbol{z})}{\partial\mathcal{M}} \tag{1}$$

This paper presents a method to compute these closed-loop sensitivities.

Equations of Aircraft Motion

It is assumed that actual aircraft trajectories are contained in the three-dimensional point-mass equations of motion for a generic commercial aircraft listed next:

$$m\dot{V}_t = T\cos\alpha_t - D - mg\sin\gamma_a - m\dot{W}_V \tag{2}$$

$$mV_t\cos\gamma_a\dot{\chi}_a = (T\sin\alpha_t + L)\sin\mu - m\dot{W}_\chi \tag{3}$$

$$mV_t\dot{\gamma}_a = (T\sin\alpha_t + L)\cos\mu - mg\cos\gamma_a + m\dot{W}_\gamma \tag{4}$$

$$\dot{x}_I = V_t\cos\gamma_a\sin\chi_a + W_x \tag{5}$$

$$\dot{y}_I = V_t\cos\gamma_a\cos\chi_a + W_y \tag{6}$$

$$\dot{h}_I = V_t\sin\gamma_a + W_h \tag{7}$$

$$\dot{m} = -\dot{m}_f(M, h_p, T) \tag{8}$$

Lift and drag are given by

$$L = \tfrac{1}{2}\rho V_t^2 S C_L, \qquad D = \tfrac{1}{2}\rho V_t^2 S C_D \tag{9}$$

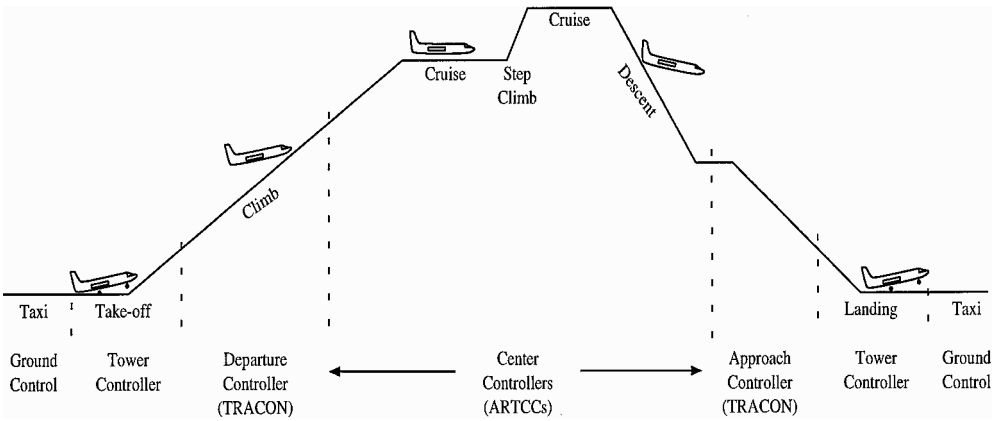

Fig. 1 Typical commercial flight procedure.

where

$$C_D = C_D(C_L, M) \tag{10}$$

Fuel flow rate is a function of Mach number, pressure altitude, and thrust as shown in Eq. (8). Wind components along the velocity vector are given by

$$\dot{W}_V \triangleq \cos\gamma_a \sin\chi_a \dot{W}_x + \cos\gamma_a \cos\chi_a \dot{W}_y + \sin\gamma_a \dot{W}_h \tag{11}$$

$$\dot{W}_\chi \triangleq \cos\chi_a \dot{W}_x - \sin\chi_a \dot{W}_y \tag{12}$$

$$\dot{W}_\gamma \triangleq \sin\gamma_a \sin\chi_a \dot{W}_x + \sin\gamma_a \cos\chi_a \dot{W}_y - \cos\gamma_a \dot{W}_h \tag{13}$$

Controllers and pilots often use variables such as Mach number, calibrated airspeed, etc., to specify flight trajectories. Relations between these variables and the state variables are given next:

$$V_{\mathrm{CAS}} = \sqrt{5} a_{\mathrm{sl}} \times \left[\left((p/p_{\mathrm{sl}}) \left\{ \left[\left(V_t^2 / 5a^2 \right) + 1 \right]^{\frac{7}{2}} - 1 \right\} + 1 \right)^{\frac{2}{7}} - 1 \right]^{\frac{1}{2}} \tag{14}$$

$$M = V_t / a \tag{15}$$

$$V_g = \sqrt{\dot{x}_I^2 + \dot{y}_I^2} \tag{16}$$

$$\tan\gamma_I = \dot{h}_I / V_g \tag{17}$$

$$\tan\chi_I = \dot{x}_I / \dot{y}_I \tag{18}$$

Elements of Solutions

Error Sources

Many error sources cause the actual trajectories to differ from the computed trajectories, as shown in Fig. 2. These error sources can be grouped into three basic categories: numerical solution errors, equation approximations, and modeling errors. 1) The use of numerical schemes such as the Runge–Kutta integration method will unavoidably introduce numerical solution errors. 2) Trajectory synthesis algorithms for CTAS and FMS must be reliable and fast, as well as sufficiently accurate. As a result, the preceding equations are simplified to achieve a balance between accuracy and computational speed. 3) Finally, trajectory synthesis uses aircraft performance models, weather models, and measurements of aircraft states. Errors in these models and measurements will be called modeling errors or external errors.

Corresponding to the three error sources, four different trajectory concepts can be defined. As shown in Fig. 3, a computed trajectory z is the output of a trajectory prediction program such as the CTAS trajectory synthesizer or an FMS. A synthesis trajectory z^* represents the ideal solution of a trajectory synthesis problem, if there are no errors in the numerical solution process. An actual trajectory x is flown by an aircraft in following the control objectives consistent with those used in the trajectory prediction. Finally, a reference trajectory x^* is generated by the three-dimensional point-mass equations of motion with the pilot/autopilot feedback actions but with no external errors. Therefore, differences between computed and synthesis trajectories reflect the effects of numerical solution errors. Differences between synthesis and reference trajectories reflect the effects of equation approximations. Finally, differences between actual and reference trajectories reflect the effects of external errors.

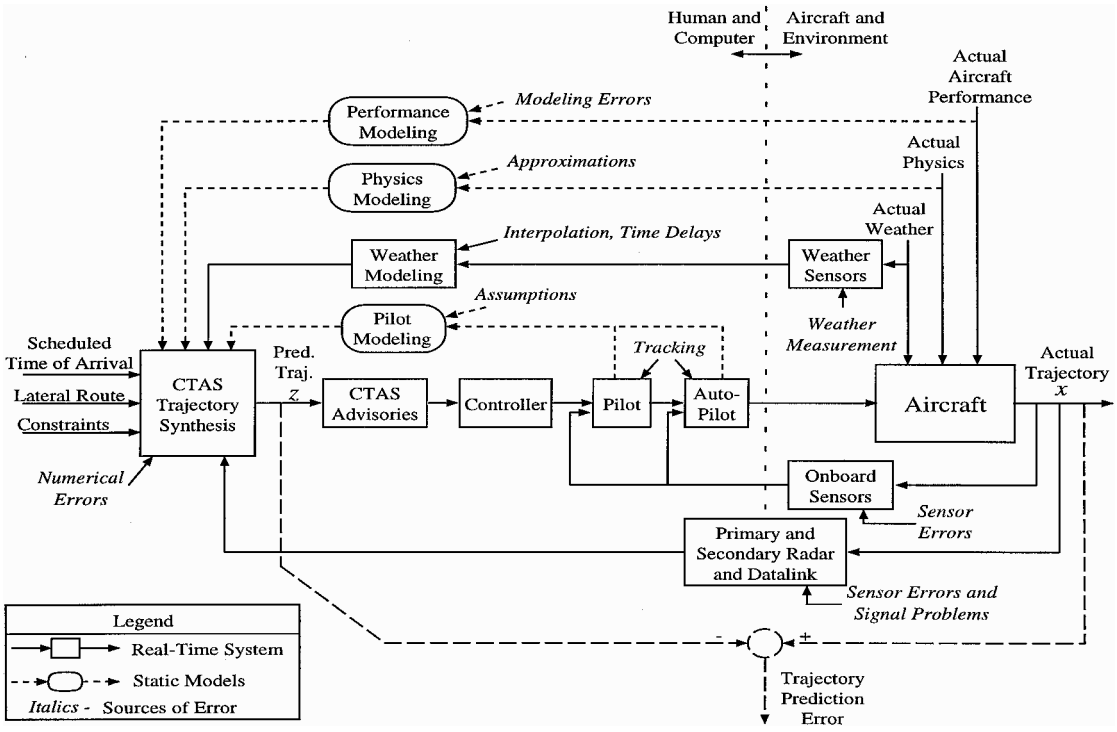

Fig. 2 Environment of CTAS trajectory synthesis.

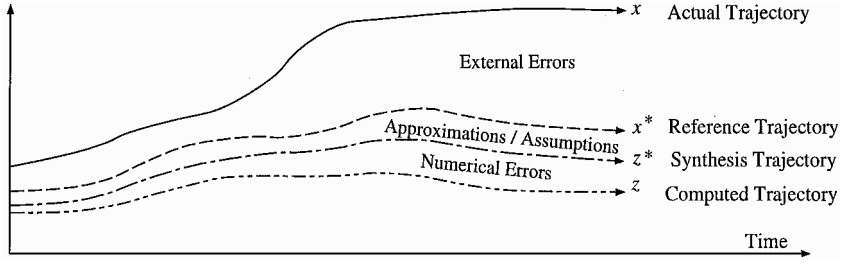

Fig. 3 Trajectory definitions.

As alluded to in Fig. 3, external errors represent the major factors that cause the actual trajectories to differ from computed trajectories[37] and are therefore the focus of the analysis method developed here. In other words, this paper determines expressions for the following closed-loop sensitivities:

$$\frac{\partial(\boldsymbol{x}-\boldsymbol{x}^*)}{\partial\mathcal{M}} \approx \frac{\partial(\boldsymbol{x}-\boldsymbol{z})}{\partial\mathcal{M}} \tag{19}$$

External errors can be mathematically expressed as either uncertain parameters $\boldsymbol{p}$ or uncertain time-varying disturbances $\boldsymbol{d}(t)$. Sometimes, a given error source is studied both as a parameter and as an input function. As a result, the dynamics of aircraft motion in Eqs. (2–8) can be expressed symbolically as

$$\dot{\boldsymbol{x}} = F[\boldsymbol{x}, \boldsymbol{u}, \boldsymbol{d}(t), \boldsymbol{p}] \tag{20}$$

where the state vector is $\boldsymbol{x} = [V_t, \chi_a, \gamma_a, x_I, y_I, h_I, m]'$ and the control vector is $\boldsymbol{u} = [T \text{ or } \kappa, C_L, \mu]'$. External errors $\boldsymbol{d}(t)$ and $\boldsymbol{p}$ will be specified later in numerical examples.

Flight Procedures and Pilot Feedback Controls

A typical commercial flight consists of a series of segments, as shown in Fig. 1. These segments can be defined by control objectives and termination conditions designed to be flyable by a pilot or an autopilot. There are three categories of vertical control objectives: 1) speed (calibrated airspeed, true airspeed, Mach, ground speed, or arrival time), 2) flight path (altitude, altitude rate, or flight-path angle), and 3) throttle control. Each vertical flight segment is defined by choosing exactly two control objectives, at most one from each category. This either explicitly or implicitly defines how the aircraft pitch and thrust are controlled. For example, choosing constant Mach and idle thrust defines a descent segment that controls speed using aircraft pitch. A certain number of flight segments can be grouped together to form predefined flight profiles. In a flight profile, each trajectory segment ends and the next segment begins when a specific scalar condition is met. These conditions are called capture conditions or termination conditions.[10] If a constant Mach segment is followed by a constant calibrated airspeed (CAS) segment, for example, the termination condition for the constant Mach segment is to reach a specified CAS. In general, termination variables can be path distance, speed, altitude, time, etc. Typically, a termination condition is one of the control objectives of the following segment as in the preceding example. Figure 4 shows one of the descent profiles used in CTAS trajectory synthesizer, called a nominal profile.

In addition to the vertical control objectives, the lateral (horizontal) motion must also be specified in one of several ways. Aircraft that are equipped with an FMS or an inertial reference system can track an inertial path along a series of waypoints. Unequipped aircraft can track inertial paths when flying to or from a very high frequency omnidirectional range station but in other cases can only fly commanded aerodynamic headings.

The control objectives are met in flight by active feedback control from either the pilot or an autopilot. Actual feedback control laws used on board aircraft are very complicated, and models of pilot control are difficult to obtain. In this paper, feedback control laws are generated using dynamic inversion or feedback linearization.[38,39] In this method, the difference between a control objective and the actual aircraft variable, called tracking error, is differentiated until a control variable appears. The number of differentiations required defines the order of the control law. Then a linear combination of the

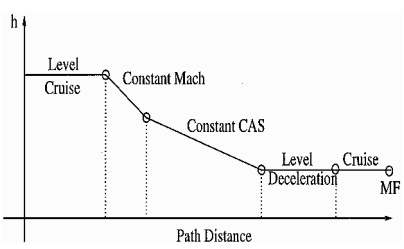

Fig. 4 Nominal descent profile.

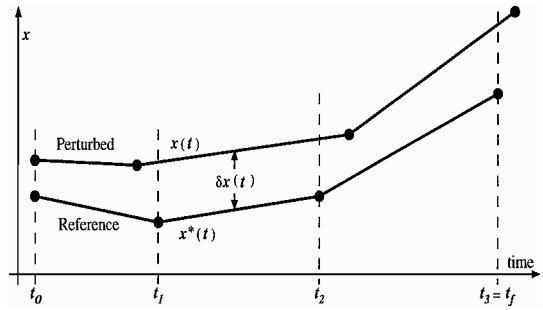

Fig. 5 Multiple-segment trajectory.

tracking error and its derivatives is formed with coefficients selected to model reasonable frequencies of response for a pilot or autopilot. For example, the objective of constant throttle can be expressed as $\kappa = \kappa_s$. Because this objective directly involves a control variable κ, the corresponding feedback control law is zeroth order and can be expressed as $G = \kappa - \kappa_s = 0$. The objective of constant Mach can be expressed as $M = M_s$. If the throttle is used to control the speed, the corresponding feedback control law will be of first order and is given by $G = \dot{M} + K(M - M_s) = 0$. If the speed is controlled by pitch, on the other hand, the corresponding control law will be of second order and is given by $G = \ddot{M} + K_1\dot{M} + K_2(M - M_s) = 0$. Symbolically, the resulting feedback control laws for a certain trajectory segment can be expressed as

$$0 = G[\boldsymbol{x}, \boldsymbol{u}, \boldsymbol{d}(t), \boldsymbol{p}] \tag{21}$$

Boundary Conditions of Trajectory Prediction

Initial conditions for trajectory prediction are determined from radar measurements or onboard navigation systems. These initial conditions are typically given in terms such as pressure altitude, Mach number, or CAS and must be converted into initial values of the state variables used in the equations of motion. As a result, the initial states are affected by external errors in the measurements. A termination condition specifies the point at which one segment connects with the next. In general, termination conditions are affected by external errors as well. Together, the boundary conditions of trajectory prediction for one segment, e.g., the first segment in Fig. 5, can be expressed as

$$0 = Q[\boldsymbol{x}(t_0), \boldsymbol{d}(t_0), \boldsymbol{p}] \tag{22}$$

$$0 = \psi[\boldsymbol{x}(t_1), \boldsymbol{d}(t_1), \boldsymbol{p}] \tag{23}$$

Closed-Loop Sensitivities

Single-Segment Trajectory

Consider the first segment in Fig. 5. Based on the preceding discussions, actual trajectories for a single trajectory segment are contained in Eqs. (20–23). These nonlinear equations can be numerically integrated to obtain a trajectory. In particular, the reference trajectory $\boldsymbol{x}^*(t)$ discussed earlier can be found by setting the external errors to zero, $\boldsymbol{d}(t) = 0$ and $\boldsymbol{p} = 0$:

$$\dot{\boldsymbol{x}}^* = F(\boldsymbol{x}^*, \boldsymbol{u}^*, 0, 0) \tag{24}$$

$$0 = G(\boldsymbol{x}^*, \boldsymbol{u}^*, 0, 0) \tag{25}$$

$$0 = Q[\boldsymbol{x}^*(t_0), 0, 0] \tag{26}$$

$$0 = \psi[\boldsymbol{x}^*(t_1), 0, 0] \tag{27}$$

Define the state variation at a fixed point in time by the difference between the perturbed trajectory and the reference trajectory (Fig. 5):

$$\delta\boldsymbol{x}(t) \triangleq \boldsymbol{x}(t) - \boldsymbol{x}^*(t) \tag{28}$$

To obtain an expression for $\delta\boldsymbol{x}(t)$, Eqs. (20) and (21) are linearized around the reference trajectory defined by Eqs. (24) and (25):

$$\delta\dot{\boldsymbol{x}} = F_x\delta\boldsymbol{x} + F_u\delta\boldsymbol{u} + F_d\boldsymbol{d} + F_p\boldsymbol{p} \tag{29}$$

$$0 = G_x\delta\boldsymbol{x} + G_u\delta\boldsymbol{u} + G_d\boldsymbol{d} + G_p\boldsymbol{p} \tag{30}$$

where

$$F_x = \left.\frac{\partial F}{\partial x}\right|_{\boldsymbol{x}=\boldsymbol{x}^*,\,\boldsymbol{u}=\boldsymbol{u}^*,\,\boldsymbol{d}=0,\,\boldsymbol{p}=0}, \qquad \text{etc.} \tag{31}$$

Based on practical flight procedures, the control laws in Eq. (21) can always be chosen so that the number of controls is equal to the number of control objectives, and G_u is invertible. As a result, Eq. (30) leads to

$$\delta\boldsymbol{u} = -G_u^{-1}[G_x\delta\boldsymbol{x} + G_d\boldsymbol{d} + G_p\boldsymbol{p}] \tag{32}$$

Substituting Eq. (32) into (29) and collecting terms, we obtain

$$\delta\dot{\boldsymbol{x}} = \bar{F}_x\delta\boldsymbol{x} + \bar{F}_d\boldsymbol{d} + \bar{F}_p\boldsymbol{p} \tag{33}$$

where

$$\bar{F}_x \triangleq F_x - F_uG_u^{-1}G_x \tag{34}$$

$$\bar{F}_d \triangleq F_d - F_uG_u^{-1}G_d \tag{35}$$

$$\bar{F}_p \triangleq F_p - F_uG_u^{-1}G_p \tag{36}$$

The initial state variation can be found by linearizing the initial measurements in Eq. (22). Because t_0 is given, $\delta\boldsymbol{x}(t_0) = d\boldsymbol{x}(t_0)$:

$$0 = Q_x\delta\boldsymbol{x}(t_0) + Q_d\boldsymbol{d}(t_0) + Q_p\boldsymbol{p} \tag{37}$$

Because the initial state conditions are determined uniquely by the measurements, the matrix Q_x must be invertible:

$$\delta\boldsymbol{x}(t_0) = -Q_x^{-1}[Q_d\boldsymbol{d}(t_0) + Q_p\boldsymbol{p}] \triangleq S_{d(t_0)}^{x(t_0)}\boldsymbol{d}(t_0) + S_p^{x(t_0)}\boldsymbol{p} \tag{38}$$

The final time of a segment can vary as the trajectory is perturbed by external errors. Because the termination condition in Eq. (23) is always satisfied at the end of a segment,

$$\mathrm{d}\psi = \psi_x\,\mathrm{d}\boldsymbol{x}(t_1) + \psi_d\,\boldsymbol{d}(t_1) + \psi_p\boldsymbol{p} = 0 \tag{39}$$

where

$$\mathrm{d}\boldsymbol{x}(t_1) \triangleq \boldsymbol{x}(t_1 + \mathrm{d}t_1) - \boldsymbol{x}^*(t_1) \approx \delta\boldsymbol{x}(t_1) + \bar{F}(t_1)\,\mathrm{d}t_1 \tag{40}$$

and

$$\bar{F} \triangleq F(\boldsymbol{x}^*, \boldsymbol{u}^*, 0, 0)|_{G(\boldsymbol{x}^*,\boldsymbol{u}^*,0,0)=0} \tag{41}$$

Substituting Eq. (40) into Eq. (39) and solving for $\mathrm{d}t_1$, we have

$$\mathrm{d}t_1 = -\dot{\psi}^{-1}[\psi_x\delta\boldsymbol{x}(t_1) + \psi_d\boldsymbol{d}(t_1) + \psi_p\boldsymbol{p}] \tag{42}$$

where $\dot{\psi} = \psi_x\bar{F}(t_1)$, and $\dot{\psi}$ is always nonzero for well-defined capture conditions.[10]

Equations (33), (38), and (42) represent a linear time-varying system that describes the variations of differences between actual and reference trajectories caused by external errors. These equations can be used to study sensitivities and worst case disturbances or to conduct covariance analysis. The derivation of terminal sensitivities is presented next.

Terminal Sensitivities

At any time t, the solution of Eq. (33) can be expressed as

$$\delta\boldsymbol{x}(t) = \Phi(t, t_0)\delta\boldsymbol{x}(t_0) + \int_{t_0}^{t}\Phi(t,\tau)\bar{F}_d(\tau)\boldsymbol{d}(\tau)\,\mathrm{d}\tau + \left[\int_{t_0}^{t}\Phi(t,\tau)\bar{F}_p(\tau)\,\mathrm{d}\tau\right]\boldsymbol{p} \tag{43}$$

where $\Phi(t, t_0)$ is the state transition matrix

$$\frac{\mathrm{d}}{\mathrm{d}t}\Phi(t, t_0) = \bar{F}_x\Phi(t, t_0), \qquad \Phi(t, t) = \boldsymbol{I}$$

Substituting Eq. (38) into Eq. (43) leads to

$$\delta\boldsymbol{x}(t) = \Phi(t, t_0)S_{d(t_0)}^{x(t_0)}\boldsymbol{d}(t_0) + \int_{t_0}^{t}\Phi(t,\tau)\bar{F}_d(\tau)\boldsymbol{d}(\tau)\,\mathrm{d}\tau + \left[\int_{t_0}^{t}\Phi(t,\tau)\bar{F}_p(\tau)\,\mathrm{d}\tau + \Phi(t, t_0)S_p^{x(t_0)}\right]\boldsymbol{p} \tag{44}$$

Of major interest are aircraft conditions at segment termination. Therefore, we need to determine sensitivities of terminal aircraft states with respect to external errors. From Eqs. (40), (42), and (44) we have

$$\mathrm{d}\boldsymbol{x}(t_1) = A_x\delta\boldsymbol{x}(t_1) - \bar{F}(t_1)\dot{\psi}^{-1}\psi_d\boldsymbol{d}(t_1) - \bar{F}(t_1)\dot{\psi}^{-1}\psi_p\boldsymbol{p} \triangleq S_{d(t_0)}^{x(t_1)}\boldsymbol{d}(t_0) + \int_{t_0}^{t_1}S_{d(\tau)}^{x(t_1)}\boldsymbol{d}(\tau)\,\mathrm{d}\tau + S_{d(t_1)}^{x(t_1)}\boldsymbol{d}(t_1) + S_p^{x(t_1)}\boldsymbol{p} \tag{45}$$

where

$$A_x \triangleq I - \bar{F}(t_1)\dot{\psi}^{-1}\psi_x \tag{46}$$

and the terminal sensitivities are defined as

$$S_{d(t_0)}^{x(t_1)} \triangleq \frac{\partial\,\mathrm{d}\boldsymbol{x}(t_1)}{\partial\boldsymbol{d}(t_0)} = A_x\Phi(t_1, t_0)S_{d(t_0)}^{x(t_0)} \tag{47}$$

$$S_{d(\tau)}^{x(t_1)} \triangleq \frac{\partial\,\mathrm{d}\boldsymbol{x}(t_1)}{\partial\boldsymbol{d}(\tau)} = A_x\Phi(t_1,\tau)\bar{F}_d(\tau) \qquad t_0 < \tau < t_1 \tag{48}$$

$$S_{d(t_1)}^{x(t_1)} \triangleq \frac{\partial\,\mathrm{d}\boldsymbol{x}(t_1)}{\partial\boldsymbol{d}(t_1)} = -\bar{F}(t_1)\dot{\psi}^{-1}\psi_d \tag{49}$$

$$S_p^{x(t_1)} \triangleq \frac{\partial\,\mathrm{d}\boldsymbol{x}(t_1)}{\partial\boldsymbol{p}} = A_x\int_{t_0}^{t_1}\Phi(t_1,\tau)\bar{F}_p(\tau)\,\mathrm{d}\tau - \bar{F}(t_1)\dot{\psi}^{-1}\psi_p + A_x\Phi(t_1, t_0)S_p^{x(t_0)} \tag{50}$$

These terminal sensitivities measure state prediction errors for when the terminal conditions are met. In particular, $S_{d(\tau)}^{x(t_1)}$ represents the sensitivity of the first segment final state to an impulsive disturbance at time τ for $t_0 < \tau < t_1$. The dimension of $S_{d_j(\tau)}^{x_i(t_1)}$ is the dimension of x_i over that of d_j, divided by time.

Multiple-Segment Trajectory

Let us use t_i, $i \in (1, 2, \ldots, f)$, to denote reference segment transition times in a multiple-segment trajectory as shown in Fig. 5, where f denotes the number of trajectory segments. In a multiple-segment trajectory, the control objectives and the terminal conditions can change discontinuously across trajectory segment boundaries. All quantities with a superscript i are valid only during the appropriate segment, $t_{i-1} \le t \le t_i$. We have, for $i = 1, 2, \ldots, f$,

$$\boldsymbol{0} = G^i[\boldsymbol{x}, \boldsymbol{u}, \boldsymbol{d}(t), \boldsymbol{p}] \tag{51}$$

$$\boldsymbol{0} = \psi^i[\boldsymbol{x}(t_i), \boldsymbol{d}(t_i), \boldsymbol{p}] \tag{52}$$

Trajectory differences around a multiple-segment reference trajectory over $[t_{i-1}, t_i]$ are governed by

$$\delta\dot{\boldsymbol{x}} = \bar{F}_x^i\delta\boldsymbol{x} + \bar{F}_d^i\boldsymbol{d}(t) + \bar{F}_p^i\boldsymbol{p} \tag{53}$$

Initial trajectory differences for the first segment are given by Eq. (38).

A key step in the analysis of a multiple-segment trajectory is determining the effects of segment transitions on error propagation. In particular, the segment transition times can themselves change. Figure 6 shows how the errors are recorded across a segment transition. Because the linear time-varying system for segment i ends at the nominal time t_i, the errors during the period between t_i and $t_i + dt_i$ must be computed based on the conditions at time t_i and changes in the segment transition time. We have from Fig. 6

$$\mathrm{d}\boldsymbol{x}(t_i) \triangleq \boldsymbol{x}(t_i + \mathrm{d}t_i) - \boldsymbol{x}^*(t_i) = \delta\boldsymbol{x}\left(t_i^-\right) + \bar{F}^i\left(t_i^-\right)\mathrm{d}t_i = \delta\boldsymbol{x}\left(t_i^+\right) + \bar{F}^i\left(t_i^+\right)\mathrm{d}t_i$$

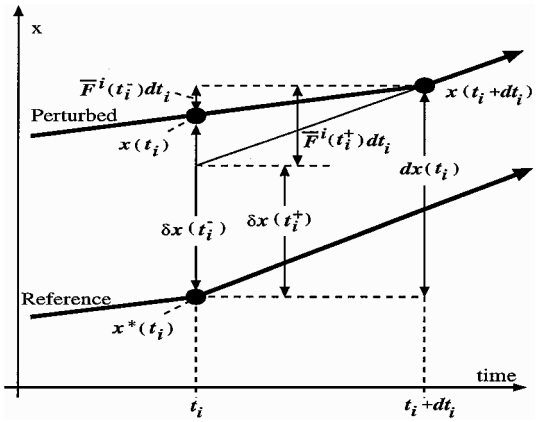

Fig. 6 Errors during segment transition.

As a result, the initial trajectory difference for segment $(i+1)$, $\delta\boldsymbol{x}(t_i^+)$, is given by

$$\delta\boldsymbol{x}\left(t_i^+\right) = \delta\boldsymbol{x}\left(t_i^-\right) + \left[\bar{F}^i\left(t_i^-\right) - \bar{F}^i\left(t_i^+\right)\right]\mathrm{d}t_i \tag{54}$$

where $\delta\boldsymbol{x}(t_i^-)$ is obtained at the end of segment i, and for $i = 1, 2, \ldots, f$,

$$\bar{F}^i\left(t_i^-\right) \triangleq F[\boldsymbol{x}^*(t_i), \boldsymbol{u}^*(t_i), 0, 0]|_{G^i[\boldsymbol{x}^*(t_i), \boldsymbol{u}^*(t_i), 0, 0]=0} \tag{55}$$

$$\bar{F}^i\left(t_i^+\right) \triangleq F[\boldsymbol{x}^*(t_i), \boldsymbol{u}^*(t_i), 0, 0]|_{G^{i+1}[\boldsymbol{x}^*(t_i), \boldsymbol{u}^*(t_i), 0, 0]=0} \tag{56}$$

$$\bar{F}^f\left(t_f^+\right) \triangleq 0 \tag{57}$$

Changes in segment transition times, for $i = 1, 2, \ldots, f$, are given by

$$\mathrm{d}t_i = -(\dot{\psi}^i)^{-1}\left[\psi_x^i \delta\boldsymbol{x}\left(t_i^-\right) + \psi_d^i \boldsymbol{d}(t_i) + \psi_p^i \boldsymbol{p}\right] \tag{58}$$

Define

$$C^i \triangleq \left[\bar{F}^i\left(t_i^+\right) - \bar{F}^i\left(t_i^-\right)\right](\dot{\psi}^i)^{-1} \tag{59}$$

Effects of segment transitions on trajectory differences can be defined through the following sensitivity functions. For $i = 1, 2, \ldots, f$,

$$S^{x(t_i^+)}_{x(t_{i-1}^+)} \triangleq \frac{\partial\delta\boldsymbol{x}\left(t_i^+\right)}{\partial\delta\boldsymbol{x}\left(t_{i-1}^+\right)} = \left[I + C^i\psi_x^i\right]\Phi^i\left(t_i^-, t_{i-1}^+\right) \tag{60}$$

$$S^{x(t_i^+)}_{d(\tau;t_i^-,t_{i-1}^+)} \triangleq \frac{\partial\delta\boldsymbol{x}\left(t_i^+\right)}{\partial\boldsymbol{d}(\tau)} = \left[I + C^i\psi_x^i\right]\Phi^i\left(t_i^-, \tau\right)\bar{F}_d^i(\tau)$$

$$t_{i-1}^+ < \tau < t_i^- \tag{61}$$

$$S^{x(t_i^+)}_{d(t_i)} \triangleq \frac{\partial\delta\boldsymbol{x}\left(t_i^+\right)}{\partial\boldsymbol{d}(t_i)} = C^i\psi_d^i \tag{62}$$

$$S^{x(t_i^+)}_{p(t_i,t_{i-1})} \triangleq \frac{\partial\delta\boldsymbol{x}\left(t_i^+\right)}{\partial\boldsymbol{p}}$$

$$= \left[I + C^i\psi_x^i\right]\int_{t_{i-1}^+}^{t_i^-} \Phi^i\left(t_i^-, \tau\right)\bar{F}_p^i(\tau)\,\mathrm{d}\tau + C^i\psi_p^i \tag{63}$$

Finally, the sensitivities of trajectory differences at the final time are defined by

$$S^{x(t_f)}_{d(\tau)} \triangleq \frac{\partial\,\mathrm{d}\boldsymbol{x}(t_f)}{\partial\boldsymbol{d}(\tau)} = \left[\prod_{j=f-1}^{i} S^{x(t_{j+1}^+)}_{x(t_j^+)}\right] \cdot S^{x(t_i^+)}_{d(\tau;t_i^-,t_{i-1}^+)}$$

$$t_{i-1} < \tau < t_i \tag{64}$$

$$S^{x(t_f)}_{d(t_i)} \triangleq \frac{\partial\,\mathrm{d}\boldsymbol{x}(t_f)}{\partial\boldsymbol{d}(t_i)} = \left[\prod_{j=f-1}^{i} S^{x(t_{j+1}^+)}_{x(t_j^+)}\right] \cdot S^{x(t_i^+)}_{d(t_i)}$$

$$t_i \in t_0, t_1, \ldots, t_f \tag{65}$$

$$S_p^{x(t_f)} \triangleq \frac{\partial\,\mathrm{d}\boldsymbol{x}(t_f)}{\partial\boldsymbol{p}} = S^{x(t_f)}_{x(t_{f-1}^+)} S^{x(t_{f-1}^+)}_{x(t_{f-2}^+)} \cdots S^{x(t_1^+)}_{x(t_0)} S_p^{x(t_0)}$$

$$+ S^{x(t_f)}_{x(t_{f-1}^+)} S^{x(t_{f-1}^+)}_{x(t_{f-2}^+)} \cdots S^{x(t_2^+)}_{x(t_1^+)} S^{x(t_1^+)}_{p(t_1,t_0)} + \cdots$$

$$+ S^{x(t_f)}_{x(t_{f-1}^+)} S^{x(t_{f-1}^+)}_{p(t_{f-1},t_{f-2})} + S^{x(t_f)}_{p(t_f,t_{f-1})} \tag{66}$$

Then the multiple-segment terminal error can be described by

$$\mathrm{d}\boldsymbol{x}(t_f) = \int_{t_0}^{t_f} S^{x(t_f)}_{d(\tau)}\boldsymbol{d}(\tau)\,\mathrm{d}\tau + \sum_{j=0}^{f} S^{x(t_f)}_{d(t_j)}\boldsymbol{d}(t_j) + S_p^{x(t_f)}\boldsymbol{p} \tag{67}$$

Equations (64–66) describe the sensitivity functions for the effects of the external errors on the final states, and Eq. (67) describes how to use the sensitivity functions to compute the terminal error for a given set of external errors. The first-order effects of moving segment transition times are embedded in these relations.

Worst Case Errors and Covariance Analysis

Equation (67) can be used to determine the worst combination of external errors that cause the largest deviation in a specified final state, such as the final time. Because the final state deviation caused by each external error source is independent in the linear expression of Eq. (67), the worst combination of external errors occur on the bounds of each error source with appropriate signs to amplify the final state deviation. In addition, the linear system defined by Eqs. (53), (38), (54), and (58) can be used to conduct covariance analysis. Compared with the classical case where only input functions are present,[40] the presence of uncertain parameters in Eq. (53) requires some special treatment.[36]

Numerical Implementations

The preceding methods are coded in C. The control laws in Eq. (51) are solved with a gradient search method to determine appropriate control actions at the current state. The initial conditions for trajectory prediction are determined from Eq. (22) using a gradient search. Differential equations are solved numerically. Before an integration step occurs, the termination condition for the current segment in Eq. (52) is checked. If the termination condition would be passed during the integration step, the time step is computed to exactly meet the termination condition. The corresponding time instants, t_i for $i = 1, 2, \ldots, f$, define the reference segment transition times. External errors cause the segment transition times in a perturbed trajectory to be different from those in the reference trajectory. For consistency, the reference segment transition times are used for the linearized system analysis and derivation of sensitivities. In particular, the state transition matrices for different segments are computed to these reference transition times.

Numerical Examples

A twin-engine Boeing 757-200 aircraft model is used for numerical studies. The Boeing 757-200 aircraft has a typical weight of 150,000 lb at the start of descent. The aerodynamic drag model for this aircraft is the same model as is used in CTAS (as of 1995). It is in the form of equilibrium trim drag as a function of lift coefficient and Mach, as given in Eq. (10). The engine model is based on the CF6-6D and is in the form of thrust and fuel flow as functions of pressure altitude, throttle setting, and air temperature.[41] The 1969 standard atmosphere is used, and average wind is assumed to be zero.

The nominal descent trajectory shown in Fig. 4 is examined in detail. This trajectory is chosen to represent a flight of 150 n mile through a center airspace to a handoff to a TRACON facility at a path distance defined as $s = 0$ for convenience. We first consider

Table 1 Nominal descent profile

Segment number	Control object 1	Control object 2	Segment terminal	End time, s
1	$h_p = \text{FL350}$	$M = 0.79$	$s_{\text{TOD}} = 79$ n mile	561.9
2	$M = 0.79$	$\dot{h}_p = -3{,}300$ fpm	$V_{\text{CAS}} = 287$ kn	629.1
3	$V_{\text{CAS}} = 290$ kn	$\kappa =$ idle	$h_b = 10{,}400$ ft MSL	1,208.9
4	$h_b = 10{,}000$ ft MSL	$\kappa =$ idle	$V_{\text{CAS}} = 250$ kn	1,264.7
5	$h_b = 10{,}000$ ft MSL	$V_{\text{CAS}} = 250$ kn	$s = 0$ n mile	1,296.5

Table 2 Terminal sensitivity to parametric disturbances

		Terminal state error				
Error source	Magnitude and units	V_t, kn	x_I, n mile	h_I, ft	Weight, lb	time, s
Weight_{ic}	7000 lb	0	0	−11	7016	−6.3
Thrust	500 lb	−0.1	0	−18	101	−10.6
Drag	5%	0.1	0	19	−101	11.0
Temp.	2°F	0.5	0	37	6	−3.5
Sea level press.	0.1 in-Hg	−0.1	0	86	−1	0.6
Tailwind	10 kn	−0.1	0	−13	70	−39.2
Vert. wind	1 kn	−0.1	0	−14	73	−7.8
V_{cmd}	2 kn CAS	2.2	0	5	−13	−1.1
M_{cmd}	0.005 nondim.	0	0	−2	−2	−5.5
$h_{p_{cmd}}$	200 ft	0.9	0	201	7	−0.6
s_{TOD}	1 n mile	0	0	5	−7	3.7
Altim. set	0.1 in-Hg	0	0	0	0	−0.1

a speed-on-pitch control method, which fixes the throttles at idle for most of the descent. This method of control is consistent with manual pilot control using the stick and throttle or using the autopilot/autothrottle. The segment terminations are specified in Table 1 and are chosen with considerations for the anticipations that the pilot or the FMS performs during segment transitions. This has the effect of switching the control laws to the next segment before the current segment terminates. If these anticipations are not performed, there will be overshoots in tracking the control objectives for some segments. Also, the initial portion of the descent (the second segment) is chosen to mimic the way a pilot gradually reduces the throttle to control speed as the descent rate increases. This is implemented by choosing as control objectives the desired speed and an inertial flight-path angle that is slightly shallower than that in an equilibrium idle descent at the desired speed. The end of the trajectory is based on position and the final segment of the trajectory is in level flight at a specified altitude. In the current examples, only the vertical flight segments are studied. The primary terminal trajectory deviations of interest are the errors in the arrival time and the final weight (fuel burn).

Figure 7 shows examples of a reference trajectory compared with a perturbed trajectory, in which actual thrust is 500 lb less than the reference thrust. Errors in altitude and Mach number gradually increase as the aircraft descends, whereas calibrated airspeed errors are well under control until toward the end. The final termination condition specifies baro-corrected altitude, path distance, and speed, and the effects of thrust errors appear in the time of arrival and final weight at the metering fix. In general, differences between perturbed and reference variables that are not directly controlled within a given segment grow as a function of time, whereas variables specified in segment control objectives stay the same in both perturbed and reference trajectories. As the aircraft transitions from one segment to another, differences in some variables transfer into differences in other variables because of the change in segment control objectives.

Table 2 lists sources of external errors considered as parametric errors and the corresponding terminal sensitivities of several state variable deviations. The sensitivity results presented in Table 2 are scaled by reasonable values of the external errors so that the relative importance of the various errors can be compared. Essentially, the results in Table 2 represent elements of the $S_p^{x(t_f)}$ matrix in Eq. (67), converted to a familiar set of units and scaled by reasonable sizes of errors.

Some of the error sources in Table 2 can also be considered as uncertain input functions, and the corresponding sensitivities are described by $S_{d(\tau)}^{x(t_f)}$ in Eq. (67). Figure 8 shows the impulsive

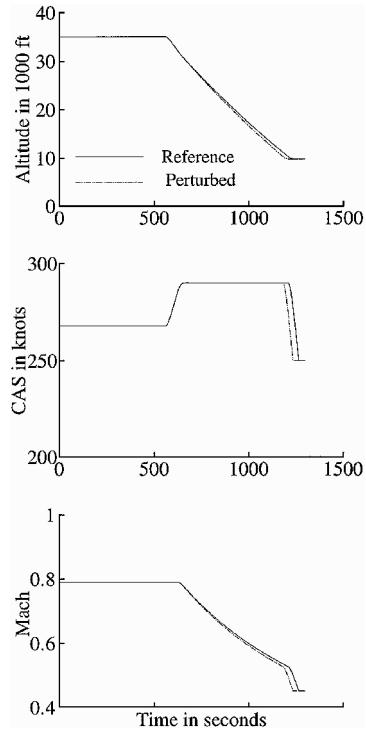

Fig. 7a Effects of a constant thrust error (− 500 lb), part A.

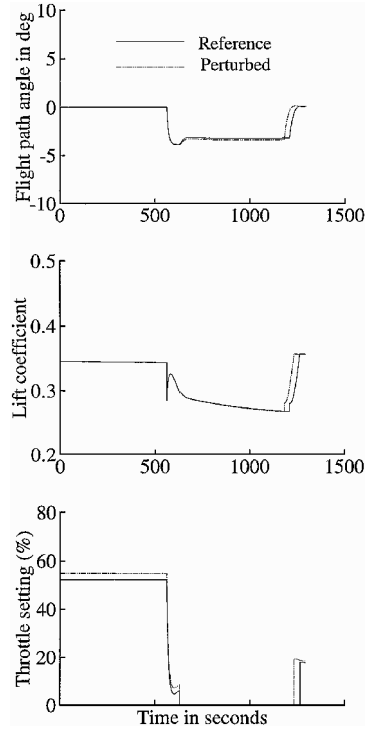

Fig. 7b Effects of a constant thrust error (− 500 lb), part B.

Table 3 Effects of control methods on final time sensitivity

Error source	Magnitude and units	Speed on pitch	Final time sensitivity (in seconds) CTAS const. proc.	FMS throttle fixed	FMS throttle free	FMS ground speed	FMS time-of-arrival control
Weight_{ic}	7000 lb	−6.3	−2.8	−9.5	−0.1	−0.8	0
Thrust	500 lb	−10.6	−4.6	−16.8	−0.3	0	0
Drag	5%	11.0	4.8	17.4	0.3	0	0
Temp.	2°F	−3.5	−3.0	−4.3	−2.6	−0.1	0
SL press.	0.1 in-Hg	0.6	0.7	0.9	0.6	0	0
Tailwind	10 kn	−39.2	−35.6	−46.6	−32.5	−1.1	−2.6
Vert. wind	1 kn	−7.8	−3.3	−12.4	−0.2	0	0
V_{cmd}	2 kn	−1.1	−2.8	−0.2	−4.4	−5.9	−0.9
M_{cmd}	0.005 nondim.	−5.5	−4.9	−6.8	−4.1	——	——
h_{pcmd}	200 ft	−0.6	−0.9	−0.7	−1.6	−0.1	0
s_{TOD}	1 n mile	3.7	2.2	——	——	——	——
Altim. set	0.1 in-Hg	−0.1	0.5	−0.6	0.6	0	0

Table 4 Worst case arrival time error

Worst case error sources	Speed on pitch	Worst case arrival time (in seconds) CTAS const. proc.	FMS throttle fixed	FMS throttle free	FMS ground speed	FMS time-of-arrival control
Parametric dist. only	93	68	119	49	9.6	3.5
Time-varying dist.	97	73	126	53	9.7	3.6

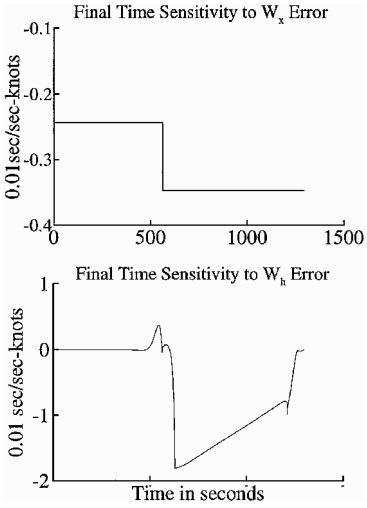

Fig. 8 Final time sensitivity to time-varying winds.

sensitivities of the final arrival time with respect to horizontal and vertical wind components. It is interesting to note that errors in horizontal wind measurements after the top of descent have a larger impact on aircraft time-of-arrival accuracy. The vertical wind acts through altitude change to affect final arrival time. As a result, the sensitivity of arrival time to vertical wind errors during the idle thrust descent decreases with altitude.

The trajectory sensitivities for several different control methods are compared in Tables 3 and 4 to the speed-on-pitch control method shown earlier. The CTAS constrained procedure is a manual procedure that is similar to the speed-on-pitch method except toward the end of the trajectory; it then models a homing procedure to meet a desired bottom-of-descent altitude constraint at a metering fix. A present day FMS uses the aircraft pitch to control the altitude along a computed path. The throttles are fixed at idle if the airspeed is close to or slightly higher than the desired speed and becomes active if the airspeed drops much below the desired speed. Two models of conventional FMSs are studied. In an FMS with fixed throttles, the throttles are assumed to be fixed during the entire descent flight. In an FMS with throttles free, it is assumed that both throttles and speed brakes can be varied to follow the reference airspeed history. In addition, two concepts of advanced FMSs are examined. The ground speed FMS controls the aircraft along a planned ground speed profile. The time-of-arrival FMS adjusts the airspeed command gradually to cross the metering fix at a desired time. The ground speed control method may not be practical for real implementations because it causes too much throttle activity and airspeed variation, but it is shown here for comparison.[36]

Table 4 shows the time-of-arrival errors caused by worst combinations of external error sources. In particular, the worst case time-of-arrival error with the speed-on-pitch control method is 97 s, assuming functional disturbances. If this is taken to be three standard deviations, we would have $\sigma = 32$ s. This is consistent with flight test results of ±20 s of arrival time accuracy.

Discussions

As shown in Table 2, the tailwind error is the most significant disturbance for time-of-arrival prediction with the speed-on-pitch control method. Actually, the tailwind affects the final time similarly for the first four control methods in Table 3 because all four methods control to airspeed. In comparison, the ground speed FMS and the time-of-arrival FMS both well reject the tailwind disturbance on final time, at the expense of fuel consumption.[36] The thrust, drag, weight, and vertical wind disturbances have moderate impact upon final time errors for the first three control types. The other three control types can reduce the sensitivities of final times to these disturbances by modulating the throttles as appropriate. The altitude-related disturbances (altitude tracking error, sea level pressure error, and altimeter setting error) have little effect on the final time error but are relevant when accurate control of altitude is important. Finally, the scaled temperature disturbance in this study does not have a significant impact on the trajectory errors. However, there are occasions when the temperature error may be much larger than 2°, such as when the location of a weather frontal system is not predicted accurately. Table 4 shows the overall effectiveness of various control methods in reducing final time sensitivity to external errors.

The selection of control methods significantly affects the distribution of trajectory errors among different state variables. The CTAS constrained procedure and the FMS throttles-free control method are similar; both aim for a desired bottom-of-descent point and have the freedom to use throttles or speed brakes. With either type of control, the time of arrival is less sensitive to external errors than with the speed-on-pitch control. The CTAS constrained procedure has larger

altitude errors than the FMS during the middle of the descent, because the former is not tracking a stored path like the FMS control types. The FMS controls the vertical path at the expense of airspeed variations. As a result, the altitude history controlled by an FMS with fixed throttles is very insensitive to errors, whereas effects of errors are pushed from the altitude to the speed and arrival time. The FMS with the throttles free is very insensitive in altitude and has less time-of-arrival sensitivity than all of the three prior control types in Table 3. The enhanced FMS trajectories with ground speed or time-of-arrival control are very insensitive in both altitude and time of arrival. On the other hand, these two control methods have higher final weight sensitivities (thus fuel weight) to some of the disturbances. In summary, all types of FMS methods control altitude very well, the FMS throttles-free method controls airspeed well, and the FMS ground speed and time-of-arrival methods both control final time well. The CTAS constrained procedure is similar to the FMS throttles-free in the vicinity of the bottom of descent, where the altitude and airspeed are well controlled.

The CTAS constrained procedure provides better control of the final arrival time than the speed-on-pitch approach. For equipped aircraft, the FMS with the throttles free provides a near-term solution for good arrival time control. Two approaches can be taken to obtain this behavior from a conventional FMS. First, the pilot can be instructed to monitor the airspeed actively during descent and to use the speed brakes to prevent speed from building up, even before the FMS puts up the message that drag is required. This effectively promotes the throttles-fixed behavior of an FMS to the throttles-free behavior. Second, the FMS descent trajectory can be computed with an off-idle throttle setting. This allows the throttles to retard some during the descent if disturbances cause an increase in energy, thus maintaining automatic control of airspeed. This method of computing a descent trajectory is already done in some FMSs in aircraft today but would require modifications to most FMSs. Also, this approach may not be practical on some aircraft because some jet engine types cannot be controlled accurately at near-idle throttle settings.

In general, the methods of trajectory prediction accuracy analysis discussed in this paper can be used in two ways. They can be used to determine which disturbances contribute the most to trajectory prediction errors and to understand which control methods are less sensitive to disturbances.

Conclusions

This paper develops an efficient method for analyzing effects of modeling errors on trajectory prediction accuracy in air traffic management and flight management systems. In particular, concepts of closed-loop sensitivities for trajectory predictions are defined as the relative changes of differences between actual and computed trajectories with respect to modeling errors in the presence of pilot/autopilot feedback control actions. Then modeling errors are treated as disturbance inputs to aircraft equations of motion and are mathematically represented as either uncertain parameters or time-varying disturbances. Pilot/autopilot feedback controls that follow flight procedures are modeled with feedback linearization. Aircraft equations of motion together with control laws are linearized along reference trajectories, and the resulting linearized system is used to obtain expressions for closed-loop sensitivities.

The method is applied to the CTAS as well as FMSs. Possible error sources in CTAS and FMSs are determined, and appropriate magnitudes of these error sources are used. Several different types of feedback control are analyzed, including speed-on-pitch control, a model of the CTAS constrained procedure, two models of conventional FMSs, and two concepts of advanced FMSs. Examples in this paper demonstrate that modeling errors manifest themselves as errors in trajectory variables. Selection of different feedback control methods affects the distribution of error effects on different variables. With the selected scales of various disturbances, the tailwind error represents the most significant disturbance to final time predictions.

The proposed method provides semianalytical expressions for closed-loop sensitivities, offers physical insight into the effects of error sources, and is computationally fast.

Acknowledgments

This work is supported by the Terminal Air Traffic Management Branch at NASA Ames Research Center under NCC2-868 and by Honeywell Technology Center. We thank Heinz Erzberger and Steve Green for many helpful discussions and Victor Cheng for help in formulating the problem.

References

[1]Erzberger, H., Davis, T. J., and Green, S., "Design of Center-TRACON Automation System," AGARD Guidance and Control Symposium on Machine Intelligence in Air Traffic Management, Berlin, May 1993.

[2]Erzberger, H., "Design Principles and Algorithms for Automated Air Traffic Management," AGARD Lecture Series No. 200 on Knowledge-Based Functions in Aerospace Systems, Madrid, Paris, and San Francisco, Nov. 1995.

[3]Denery, D. G., and Erzberger, H., "The Center-TRACON Automation System: Simulation and Field Testing," NASA TM 110366, Aug. 1995.

[4]Davis, T. J., Erzberger, H., Green, S. M., and Nedell, W., "Design and Evaluation of Air Traffic Control Final Approach Spacing Tool," *Journal of Guidance, Control, and Dynamics,* Vol. 14, No. 4, 1991, pp. 848–854.

[5]Davis, T. J., Krzeczowski, K. J., and Bergh, C., "The Final Approach Spacing Tool," 13th International Federation of Automatic Control Symposium on Automatic Control in Aerospace, Palo Alto, CA, Sept. 1994.

[6]Erzberger, H., and Tobias, L., "A Time-Based Concept for Terminal-Area Traffic Management," NASA TM 88243, April 1986.

[7]Erzberger, H., and Chapel, J. D., "Concepts and Algorithms for Terminal-Area Traffic Management," *Proceedings of the American Control Conference* (San Diego, CA), American Automatic Control Council, Evanston, IL, 1984, pp. 166–173.

[8]Erzberger, H., "Automation of On-Board Flightpath Management," NASA TM 84212, Dec. 1981.

[9]Slattery, R. A., and Zhao, Y., "Trajectory Synthesis in Air Traffic Automation," *Journal of Guidance, Control, and Dynamics*, Vol. 20, No. 2, 1997, pp. 232–238.

[10]Zhao, Y., and Slattery, R. A., "Capture Conditions for Merging Trajectory Segments to Model Realistic Aircraft Descents," *Journal of Guidance, Control, and Dynamics*, Vol. 19, No. 2, 1996, pp. 453–460.

[11]Krzeczowski, K., Davis, T. J., Erzberger, H., Lev-Ram, I., and Bergh, C., "Knowledge-Based Scheduling of Arrival Aircraft," *Proceedings of the AIAA Guidance, Navigation, and Control Conference* (Baltimore, MD), AIAA, Washington, DC, 1995.

[12]Robinson, J., Davis, T. J., and Issacson, D. R., "Fuzzy Reasoning-Based Sequencing of Arrival Aircraft in the Terminal Area," *Proceedings of the AIAA Guidance, Navigation, and Control Conference* (New Orleans, LA), AIAA, Reston, VA, 1997.

[13]Issacson, D. R., Davis, T. J., and Robinson, J., "Knowledge-Based Runway Assignment for Arrival Aircraft in the Terminal Area," *Proceedings of the AIAA Guidance, Navigation, and Control Conference* (New Orleans, LA), AIAA, Reston, VA, 1997.

[14]Slattery, R. A., and Green, S., "Conflict-Free Trajectory Planning for Air Traffic Control Automation," NASA TM 108790, Jan. 1994.

[15]Bergh, C. P., Krzeczowski, K. J., and Davis, T. J., "TRACON Aircraft Arrival Planning and Optimization Through Spatial Constraint Satisfaction," *Air Traffic Control Quarterly*, Vol. 3, No. 2, 1995, pp. 117–138.

[16]Erzberger, H., and Lee, H. Q., "Constrained Optimal Trajectories with Specified Range," *Journal of Guidance and Control*, Vol. 3, No. 1, 1980, pp. 78–85.

[17]Sorenson, J. A., and Waters, M. H., "Airborne Method to Minimize Fuel with Fixed Time-of-Arrival Constraints," *Journal of Guidance and Control*, Vol. 4, No. 3, 1981, pp. 348, 349.

[18]Burrows, J. W., "Fuel-Optimal Aircraft Trajectories with Fixed Arrival Times," *Journal of Guidance, Control, and Dynamics*, Vol. 6, No. 1, 1983, pp. 14–19.

[19]Chakravarty, A., "Four-Dimensional Fuel-Optimal Guidance in the Presence of Winds," *Journal of Guidance, Control, and Dynamics*, Vol. 8, No. 1, 1985, pp. 16–22.

[20]Liden, S., "Practical Considerations in Optimal Flight Management Computations," *Journal of Guidance, Control, and Dynamics*, Vol. 9, No. 4, 1986, pp. 427–432.

[21]Williams, D. H., "Impact of Mismodeled Idle Engine Performance on Calculation and Tracking of Optimal 4-D Descent Trajectories," *Proceedings of the American Control Conference* (Seattle, WA), American Automatic Control Council, Evanston, IL, 1986, pp. 681–686.

[22]Williams, D. H., "Fuel Penalties and Time Flexibility of 4D Flight Profiles Under Mismodeled Wind Conditions," NASA TM 89128, March 1987.

[23]Williams, D. H., and Knox, C. E., "4D Descent Trajectory Generation Techniques Under Realistic Operating Conditions," *Aircraft Trajectories, Computations–Predictions–Control*, Vol. 2, Air Traffic Handling and

Ground-Based Guidance of Aircraft, AGARD-AG-301, Vol. 2, May 1990, pp. 25-1–25-22.

[24]Hunter, G., and Bortins, R., "CTAS Error Sensitivity Study: Analysis Plan," Seagull Technology, Inc., TM 95133-02, Los Gatos, CA, June 1995.

[25]Couluris, G. J., Weidner, T., and Sorenson, J. A., "Initial Air Traffic Management (ATM) Enhancement Potential Benefits Analysis," Seagull Technology, Inc., TM 95151-01, Los Gatos, CA, Sept. 1996 (report to the FAA under Contract DTFA01-96-Y-01009).

[26]Couluris, G. J., Weidner, T., and Sorenson, J. A., "Final Approach Enhancement and Descent Trajectory Negotiation Potential Benefits Analysis," Seagull Technology, Inc., TM 95142-02, Los Gatos, CA, July 1997 (report to NASA Ames Research Center under Contract NAS2-13767).

[27]Hunter, G., and Bortins, R., "Effects of Storm Forecasting Errors on Air Traffic Control Automation System Performance," Seagull Technology, Inc., TM 95129-01, Los Gatos, CA, Feb. 1995 (report to the FAA under Contract DTFA01-94-C-01041).

[28]Hunter, G., Weidner, T., Couluris, G., Sorenson, J. A., and Bortins, R., "CTAS Error Sensitivity, Fuel Efficiency, and Throughput Benefits Analysis," Seagull Technology, Inc., TM 95150-02, Los Gatos, CA, July 1996 (report to the FAA under Contract DTFA01-94-Y-01046, Task 2).

[29]Green, S., and Vivona, R., "Field Evaluation of Descent Advisor Trajectory Prediction Accuracy," AIAA Paper 96-3764, July 1996.

[30]Oseguera, R. M., and Williams, D. H., "Flight Evaluation of the CTAS Descent Advisor Trajectory Prediction," *Proceedings of the American Control Conference* (Seattle, WA), American Automatic Control Council, Evanston, IL, 1995, pp. 3435–3439.

[31]Izumi, K. H., "Sensitivity Studies of 4D Descent Strategies in an Advanced Metering Environment," *Proceedings of the American Control Conference* (Seattle, WA), American Automatic Control Council, Evanston, IL, 1986, pp. 687–692.

[32]Chatterji, G., Sridhar, B., and Bilimoria, K., "En-Route Flight Trajectory Prediction for Conflict Avoidance and Traffic Management," AIAA Paper 96-3766, Aug. 1996.

[33]Bolender, M. A., "Assessment of CTAS ETA Prediction Capabilities," Report to NASA Ames Research Center under NASA Cooperative Agreement NCC2-669, Nov. 1994.

[34]Williams, D. H., and Green, S. M., "Airborne Four-Dimensional Flight Management in a Time-Based Air Traffic Control Environment," NASA TM 4249, March 1991.

[35]Morton, B., "Dispersion Analysis of Propulsion System Performance in Ascent-to-Orbit Missions," AIAA/ASME/SAE/ASEE 25th Joint Propulsion Conf., Paper A89-2342, Monterey, CA, July 1989.

[36]Jackson, M. R. C., "Sensitivity of Trajectory Prediction in Air Traffic Management and Flight Management Systems," Ph.D. Dissertation, Dept. of Aerospace Engineering and Mechanics, Univ. of Minnesota, Minneapolis, MN, Dec. 1997.

[37]Schubert, M., "Arrival and Departure Traffic Management Within the Terminal Area," AIAA Paper 96-3720, Aug. 1996.

[38]Slotine, J.-J. E., and Li, W.-P., *Applied Nonlinear Control*, Prentice–Hall, Englewood Cliffs, NJ, 1991, Chap. 6.

[39]Lane, S. H., and Stengel, R. F., "Flight Control Design Using Nonlinear Inverse Dynamics," *Automatica*, Vol. 24, No. 4, 1988, pp. 471–483.

[40]Bryson, A. E., and Ho, Y.-C., *Applied Optimal Control*, Hemisphere, New York, 1976, Chap. 12.

[41]Gwartney, J. D., and Shvarts, A., "A User's Guide to the Engine Model for CTAS," Seagull Technology, Inc., TM 92119-04, Los Gatos, CA, June 1992.